Journal of Catalysis 385 (2020) 194–203

Contents lists available at ScienceDirect

Journal of Catalysis

journal homepage: www.elsevier.com/locate/jcat

Enhancement of the catalytic activity of Pd nanoparticles in Suzuki coupling by partial functionalization of the reduced graphene oxide support with *p*-phenylenediamine and benzidine

Amr Awad Ibrahim [a,b], Andrew Lin [a], Mina Shawky Adly [a,b], M. Samy El-Shall [a,*]

[a] Department of Chemistry, Virginia Commonwealth University, Richmond, VA 23284-2006, United States
[b] Department of Chemistry, Faculty of Science, Mansoura University, Al-Mansoura 35516, Egypt

ARTICLE INFO

Article history:
Received 14 February 2020
Revised 12 March 2020
Accepted 13 March 2020

Keywords:
Suzuki cross coupling
Heterogeneous catalysis
Pd nanoparticles
Chemically modified graphene oxide
Strong electrostatic adsorption

ABSTRACT

This paper reports the development of novel supports for highly active Pd nanoparticles for room temperature Suzuki cross coupling reactions. The partial functionalization of the reduced graphene oxide support by the N-containing *p*-phenylenediamine and benzidine molecules results in the dispersion of small Pd nanoparticles in the solid catalysts Pd/(RGO-PPD) and Pd/(RGO-BZD) which demonstrate excellent catalytic activity for Suzuki coupling under ligand-free ambient conditions with unusual catalytic activity that matches that of the best homogeneous Pd catalysts. They offer remarkable turnover frequencies (400,000 h^{-1}) observed in the microwave-assisted Suzuki cross coupling reaction with easy removal from the reaction mixture, recyclability with no loss of activity, and significantly better performance than most of the reported heterogeneous Pd catalysts. The findings illustrate the exciting opportunities presented by the chemically partially functionalized reduced graphene oxide support for a variety of metallic and bimetallic catalysts for carbon-carbon bond forming reactions.

1. Introduction

It is well accepted, although not always understood, that the catalytic performance of metal nanoparticle catalysts can be strongly influenced by interaction with the support material. For example, the relatively weak interaction between metal nanoparticles and the carbon-based support materials could allow for tailoring the catalysts' properties by modification of the chemical and physical characteristics of the carbon materials [1–3]. In addition to providing a high surface area for the dispersion of the catalyst, the carbon support can also influence the catalytic reaction since it could interact differently with certain reactants or products.

The palladium-catalyzed Suzuki (or the Suzuki-Miyaura) cross-coupling reaction provides a good case study for the influence of the carbon-based support on the catalytic activity and efficient recycling of the catalyst [4–7]. A variety of carbon-based supports have been utilized for mobilizing Pd nanoparticles for cross-coupling reactions including activated carbon, carbon nanotubes, graphene oxide, reduced and partially reduced graphene oxides (RGO and PRGO, respectively) [8–18].

In addition to the unique properties of RGO and PRGO, structural defects can provide nucleation sites for the formation and anchoring of the metal nanoparticles on the surface of the RGO or PRGO nanosheets [9–11,13–15,19,20]. The presence of structural defects and remaining oxygen functional groups on the RGO or PRGO nanosheets can also influence the dispersion of the supported metal nanoparticles, modify the intrinsic reactivity and play a critical role in stabilizing the metal nanoparticles [1–3,13–15,19–26]. Chemical functionalization of the RGO support can also influence catalyst-support interaction and consequently, the activity of the supported catalysts. For example, covalent functionalization of GO by aromatic amines can result in reducing or partially reducing GO thus restoring or partially restoring the sp^2 domains responsible for conductivity [27–29]. It can also enhance the strong electrostatic adsorption (SEA) of the cationic Pd precursors through complexation with the amine or the amide groups of the functionalized support which could improve the dispersion of the Pd nanoparticles formed after the reduction of the Pd ions [30–32].

Herein, we report that partial functionalization of the RGO support by the covalent attachment of the aromatic amines p-phenylenediamine (PPD) or benzidine (BZD) results in a significant enhancement of the activity of the Pd nanoparticles in the solid Pd/(RGO-PPD) or Pd/(RGO-BZD) catalysts for the Suzuki coupling reactions with unprecedented catalytic activity that matches

* Corresponding author.
E-mail address: mselshal@vcu.edu (M.S. El-Shall).

https://doi.org/10.1016/j.jcat.2020.03.011
0021-9517/

that of the best homogeneous Pd catalysts. We demonstrate that the partial functionalization of GO with PPD or BZD molecules leaves many oxygen-bearing groups such as alcohol, and carboxylic groups intact leading to only partial reduction of the GO nanosheets. The presence of the oxygen and nitrogen groups on the surface of the partially reduced and partially functionalized GO with the aromatic amines leads to SEA of the cationic palladium precursor on the chemically modified GO support [30–32]. This strategy leads to the formation of well-dispersed Pd nanoparticles anchored on the surface of the chemically modified GO support. This concept is introduced and verified in the present paper which demonstrates that partially functionalized RGO sheets with the aromatic amines PPD or BZD are superior supports to the RGO sheets alone for the dispersion of small Pd nanoparticles that exhibit a remarkable and unprecedented enhancement of the catalytic activity of Suzuki coupling reactions.

2. Experimental section

2.1. Chemicals

All listed chemicals were purchased and used without further purification. Hydrazine hydrate was acquired from Acros Organic. Bromobenzene and graphite powder (99.999%) was supplied by Alfa Aesar. Benzidine, 30% hydrogen peroxide (H_2O_2), phenylboronic acid, *p*-phenylenediamine, potassium carbonate (K_2CO_3), potassium permanganate ($KMnO_4$), sodium nitrate, and tetraamine palladium nitrate ($Pd(NO_3)_2(NH_3)_4$) were purchased from Sigma-Aldrich.

2.2. Synthesis of functionalized graphene oxide

In the experiments, GO was prepared by the oxidation of high purity graphite powder (99.999%, 200 mesh, Alfa Aesar) according to the method of Hummers and Offeman [33]. 115 ml of H_2SO_4 was chilled to 0 °C in an ice bath with stirring and 2.5 g of crushed $NaNO_3$ was added. After 20 min, 5 g of graphite powder was added followed by the slow addition of 15 g of $KMnO_4$. After 20 min, the ice bath was removed and the mixture was maintained at 32–38 °C for 3 h with vigorous stirring. Afterwards, 230 ml of warm DI water was added and the temperature of 80 °C was maintained for 30 min as the solution turned brown. 700 ml of DI water was added followed by 8 ml of 30% H_2O_2 and the solution color turned to light gold. The synthesized GO was washed with 5 l of hot DI water and dried over three days at 60 °C. To prepare the functionalized GO support, 100 mg of GO was dispersed in 60 ml of DI H_2O with either 0.025–6.0 mmol (3–600 mg) of *p*-phenylenediamine (GO-PPD) or 0.025–0.5 mmol (4–85 mg) of benzidine (GO-BZD). The mixture was sealed in a 100 ml capacity autoclave reactor and heated at 95 °C over the course of 24 h. The recovered support was centrifuged, washed with DI water and dried overnight at 80 °C. The support materials used are denoted as GO, GO-PPD (0.025–6.0 mmol), and GO-BZD (0.025–0.5 mmol).

2.3. Catalyst preparation

20 mg of the support GO, GO-PPD (0.025–6.0 mmol) or GO-BZD (0.025–0.5 mmol) was dispersed in 15 ml of DI H_2O and sonicated to ensure dispersion. After measurement of the initial pH of the solution, 0.05 mM NH_4OH was added to increase the pH of support solution to 10.0. $[Pd(NH_3)_4]^{2+}$ solution was added to each support to achieve a target of 3 wt% Pd, followed by microwave irradiation (MWI 2.45 MHz, 300 W, 5 min) in the presence of 33 μl of hydrazine hydrate. The supported catalysts were centrifuged twice with water and twice with ethanol at 10,000 rpm followed by overnight drying at 80 °C.

2.4. Characterization techniques

Powder X-ray diffraction patterns were measured using the PANalytical MPD X'Pert PRO diffractometer with voltage 45 kV and current 40 mA via the Ni-filtered Cu kα_1 radiation with a scan speed of 2.5° 2θ/min. FTIR spectra were collected with a Thermo Scientific Nicolet iS50 FT-IR using KBr pellets. X-ray photoelectron spectroscopy (XPS) spectra of the samples were obtained using the ThermoFisher Scientific ESCALAB 250 with a microfocused monochromated AlKα X-ray source (15 kV) and a double-focusing full 180° spherical sector electron analyzer. TEM images were obtained using the Jeol JEM-1230 Transmission Electron Microscope with the Gatan Orius SC1000 side mount CCD camera at 120 kV. The palladium contents (wt.%) of the supported catalysts were measured using the Varian Vista-MPX Inductively Coupled Plasma Optical Emission Spectrometer (ICP-OES) with an Ar^+ ion plasma gas equipped with a charged-couple detector (CCD) for simultaneous detection. The reaction products were analyzed using an Agilent A 6890 N GC equipped with an HP-5MS column and a flame ionization detector used to separate and quantify the conversion of reactants into products.

2.5. Suzuki cross coupling reaction

4.1 mg of the catalyst was dispersed in 5 ml of 50% ethanol–water mixture. 0.32 mmol bromobenzene (34 μl) and 0.38 mmol phenylboronic acid (47 μl) were added to the solution and briefly sonicated to ensure good dispersion of reactants. 133 mg of K_2CO_3 was then dissolved and the solution was stirred at room temperature at 500 rpm. For the 0.03 or the 0.007 Pd mol% reactions, 590 μl or 140 μl of this solution, respectively was diluted to 4 ml of 50% ethanol–water mixture and placed in the microwave reaction tube. The reaction was run at 80 °C for 1, 2 or 5 min in a sealed 10 ml tube under microwave irradiation (CEM Discover Microwave, 300 W, 2.45 MHz). The CEM Discover Microwave Reactor allows highly accurate IR temperature control for up to 300 °C. The reaction time can be controlled in intervals from 10 s up to 10 min. The reaction progress was monitored by GC–MS and the biphenyl product was extracted with ethyl acetate via centrifugation and characterized. The catalysts were also evaluated at room temperature under similar conditions. For the room temperature reactions, small aliquots of the solution were drawn at predetermined intervals and analyzed by GC-FID to determine the conversion percentage of reactants into the biphenyl product.

3. Results

3.1. Characterization of the supported catalysts

The reactions between the amino groups of PPD (or BZD) and the epoxy and carboxylic groups of GO result in the formation of C-NH-C and CO-NH bonds due to the chemical grafting of PPD (or BZD) to the GO surface via nucleophilic substitution and condensation reactions, respectively [26–29]. Since both PPD and BZD are aromatic electron donors, they can also act as reducing agents for GO [26–29]. These aromatic amines are typically added in excess to ensure full reduction of GO since the complete removal of surface oxygen groups is desirable for electrochemical applications [26–29]. In the present work, partial functionalization of GO by PPD and BZD is required since our hypothesis is that the presence of both N- and O- containing functional groups will enhance the strong electrostatic adsorption of the Pd cations and

consequently, the dispersion of the Pd nanoparticle catalysts on the partially functionalized RGO-PPD and RGO-BZD supports as it will be demonstrated below.

Fig. 1 displays the FTIR spectra of GO, GO-0.1 PPD (0.1 mmol PPD) and GO-0.1 BZD (0.1 mmol BZD). The spectrum of GO shows the characteristic stretching vibrations of the COOH groups (C═O), the O—H deformations of the C—OH groups and C—O—C stretching vibrations at 1736 cm^{-1}, 1383 cm^{-1} and 1052 cm^{-1}, respectively, in addition to a weak band due to the epoxide group at 1220 cm^{-1} [10,34]. After functionalization by either PPD or BZD, the carbonyl and alkoxy bands are retained but slightly reduced in intensity, whereas the epoxy bands at 1052 cm^{-1} and 1220 cm^{-1} and deformation of the O—H bond of CO—H at 1383 cm^{-1} disappear indicating partial reduction of GO by the aromatic amine groups of PPD or BZD. The peak at 1573–1578 cm^{-1} is assigned to the stretching vibration of N-H in —C—NH_2 groups which is a direct consequence of the attachment of new nitrogen-containing groups into GO [26]. Additionally, the peak at 1184 cm^{-1} is assigned to the stretching vibration of the C—N—C mode in the functionalized GO by BZD [27]. Also, the small peaks at 818 cm^{-1} and 953 cm^{-1} in the spectrum of GO-BZD are assigned to the bending vibration of the C-NH group and the wagging modes of –NH group in the C-NH chemical bond consistent with previous findings [26–28]. Figs. S1A and S1B (Supplementary Materials) display the FTIR spectra of GO-PPD and GO-BZD for different concentrations of PPD or BZD used in the functionalization of GO. In both cases, the peaks associated with the N-containing functional groups at 1184 cm^{-1} and 813–818 cm^{-1} greatly increase in intensity by increasing the concentration of PPD or BZD indicating that the degree of functionalization of GO increases by increasing the contents of PPD or BZD in the reaction mixture.

The strong electrostatic adsorption (SEA) technique was employed for the adsorption of cationic $[(Pd(NH_3)_4]^{2+}$ salt to the negatively charged surface of GO [31,32]. SEA theory implies that an aqueous solution will induce a partial positive or a partial negative charge on the surface of any dispersed oxygen-laden material, such as graphene oxide, according to the material's point of zero charge (PZC) corresponding to the pH at which the surface charge of the dispersed material is at equilibrium with the solution [35,36]. If the pH of the aqueous solution is adjusted to pH 10 and supersedes the PZC of GO (GO PZC = pH 3.3–3.8) [37], the aqueous solution acts as a base relative to the surface of GO and more hydroxide interactions than proton interactions occur on the surface, leading to an abundance of O^- groups on GO [38]. The partial negative charge on the surface of GO assists towards the adsorption or uptake of cationic salts prior to reduction.

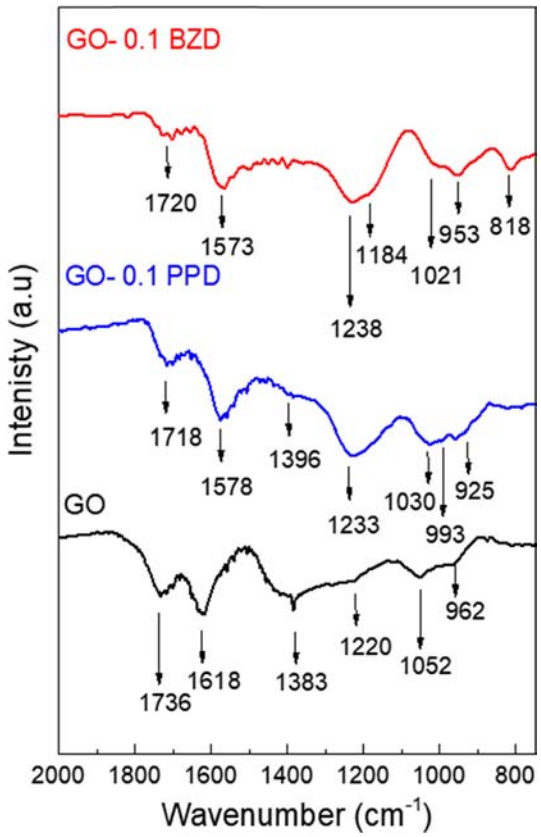

Fig. 1. FTIR spectra of GO, GO-0.1 mmol PPD and GO-0.1 mmol BZD.

The XPS spectra of the C1s and Pd3d electrons in the Pd/(RGO), Pd/(RGO-0.1 PPD) and Pd/(RGO-0.1 BZD) catalysts are displayed in Fig. 2. It is evident from the survey scan, shown in Fig. 2(A), that the peak for the nitrogen 1 s electron at approximately 399 eV is clearly present in the spectra of the Pd/(RGO-0.1 PPD) and Pd/(RGO-0.1 BZD) catalysts but not in the spectrum of the Pd/(RGO) catalyst. The atomic % of oxygen decreases from 41.2% in the Pd/(RGO) catalyst to 32.0% and 32.8% in the Pd/(RGO-0.1 PPD) and Pd/(RGO-0.1 BZD) catalysts, respectively consistent with the reduction of GO after the functionalization with PPD and BZD resulting in 7.8% and 5.1% N contents, respectively.

Fig. 2 (B) displays the C1s spectra for the Pd/(RGO-0.1 PPD), Pd/(RGO-0.1 BZD) and Pd/(RGO) catalysts which clearly indicate the presence of the sp^2 hybridized C═C bonds at (284.6 eV), C—O bonds (286.2 eV), and C═O bonds (288.8 eV) [9,10,40]. After functionalization with PPD and BZD, the 286.2 eV C—O and O—C═O peaks are severely diminished and a new shoulder at 285.1 eV corresponding to C-N bonding becomes prominent in the spectra of the Pd/(RGO-0.1 PPD) and Pd/(RGO-0.1 BZD) catalysts [27]. This offers further evidence of the substitution of surface-bound oxygen groups with the amine moieties.

Fig. 2 (C) displays the XPS spectra of the Pd-3d electron in the Pd/(RGO-0.1 PPD), Pd/(RGO-0.1 BZD) and Pd/(RGO) catalysts. The binding energy values of 335.5 and 340.8 eV corresponding to the $3d_{5/2}$ and $3d_{3/2}$ of metallic palladium, respectively are observed at higher energy values by 0.3–0.5 eV in the Pd/(RGO-0.1 PPD) and Pd/(RGO-0.1 BZD) catalysts suggesting electron transfer from palladium to the functionalized supports RGO-PPD and RGO-BZD [15]. The data show that the Pd(0)% increases from 27% to 31% and 37%, in the Pd/(RGO-0.1 PPD), Pd/(RGO-0.1 BZD) and Pd/(RGO) catalysts, respectively). It is known that the oxidation state of palladium cycles between Pd(II) and Pd(0) in the palladium-catalyzed Suzuki cross coupling reaction between the oxidative addition of a halide-bearing aryl group and the reductive elimination [41], and that Pd(0) is required to initiate oxidative addition step [42,43]. It is also established that a higher ratio of Pd(0) in the supported catalysts would usually result in higher conversion kinetics [44]. This point will be further discussed below.

Fig. 3 displays the XRD patterns of GO and the partially functionalized RGO-PPD and RGO-BZD supports with different degrees of functionalization. The GO peak at $2\theta = 11.3°$ corresponds to a *d*-spacing of 7.8 Å resulting from the insertion of hydroxyl and epoxy groups between the oxidized graphene sheets [9,34]. With the inclusion of a small amount (0.025 mmol) of *p*-phenylene diamine (Fig. 3A) or benzidine (Fig. 3B), a small upshift in the XRD peak of GO (from $2\theta = 11.3°$ to 13.1° or 13.3°) is observed. This could be attributed to restacking of the GO sheets due to partial loss of non-carboxylic acid groups [45], and also due to the partial reduction and partial functionalization of GO resulting in non-uniform d-spacing [28]. A decrease in the d-spacing from 0.78 nm to 0.66 nm implies the removal of oxygen group spacers without sufficient aromatic amines molecules to act as replacement scaffolding groups, which could result in partial restacking

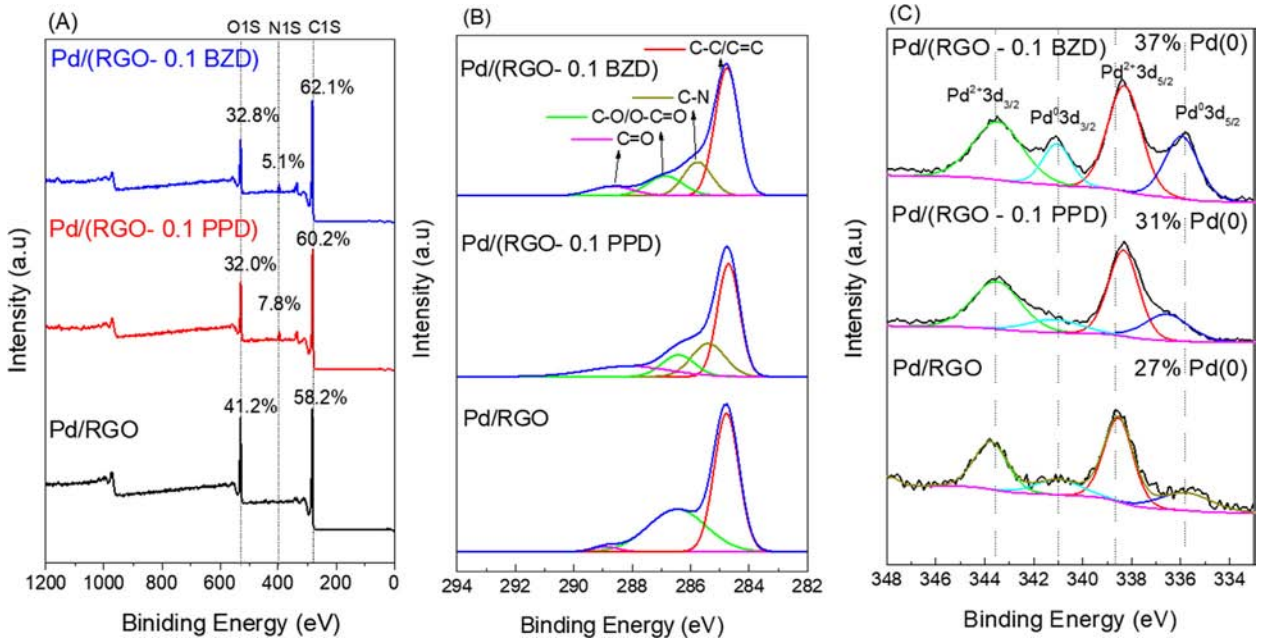

Fig. 2. (A) XPS survey, (B) high-resolution XPS spectra of C1s and (C) high-resolution spectra of Pd3d for the Pd/RGO, Pd/RGO-0.1 PPD and Pd/RGO-0.1BZD catalysts.

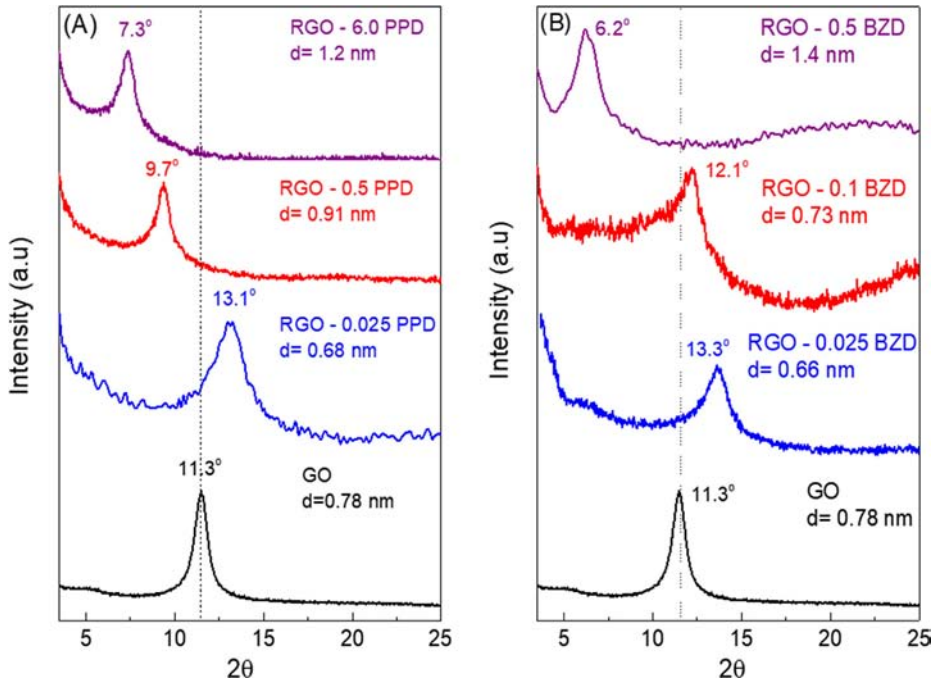

Fig. 3. XRD patterns of GO and RGO-PPD and RGO-BZD functionalized with different amounts of (A) *p*-phenylenediamine (PPD) and (B) benzidine (BZD).

of the graphitic layers. However, Fig. 3(A) and (B) show that the d_{001} peak of GO shifts to smaller 2θ values with the increased incorporation of PPD and BZD as previously reported when GO is fully reduced by the aromatic amines [26]. For example, the d_{001} peak shifts to 7.3° (d-spacing = 1.2 nm) or to 6.2° (d-spacing = 1. 4 nm) as the amount of PPD or BZD is increased to 0.6 mmol or 0.5 mmol, respectively.

Fig. 4 displays TEM images of the supported catalysts Pd/RGO, Pd/(RGO-0.025 BZD), Pd/(RGO-0.025PPD), Pd/(RGO-0.1BZD), Pd/(RGO-0.1PPD), and Pd/(RGO-0.5 BZD). The size distributions of the Pd nanoparticles determined from the TEM micrographs are shown in Fig. S2 (Supplementary Materials). At low concentrations of the PPD and BZD functional groups (0.025 mmol), the palladium size distributions are 2.9 ± 0.7 nm for the RGO- 0.025 PPD catalyst and 2.2 ± 1.1 nm for the RGO-0.025 BZD catalyst. For the RGO-BZD support, the Pd nanoparticle size starts to drastically increase as a function of the higher BZD content. As the BZD content increases from 0.025 to 0.1 to 0.5 mmol, the Pd particle size increases from 2.2 ± 1.1 to 6.6 ± 5.6 to 11.9 ± 19.9, respectively. It is also clear from Fig. 4 that the aggregation of Pd nanoparticles on the RGO-0.5 BZD support becomes highly evident.

The TEM results clearly establish that partial covalent functionalization of GO with PPD or BZD leads to significantly smaller (~3 nm) and more dispersed Pd nanoparticles as compared to the

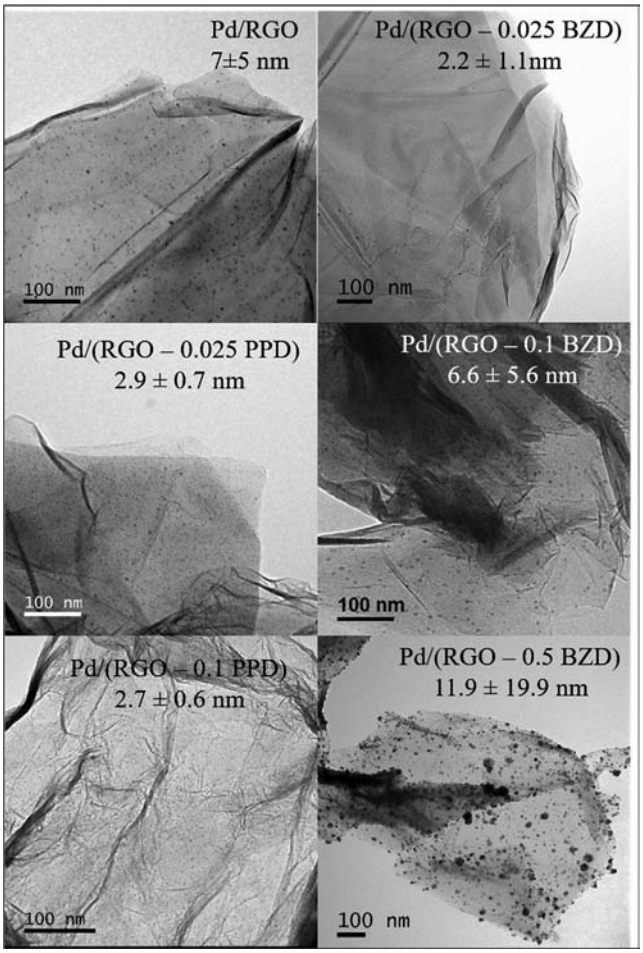

Fig. 4. TEM images of the Pd/RGO, Pd/RGO-0.025PPD, Pd/RGO-0.1PPD, Pd/RGO-0.025BZD, Pd/RGO-0.1BZD, and Pd/RGO-0.5BZD catalysts. The Pd loadings (wt%) in these catalysts, as determined by ICP-MS, are 3.5, 2.3, 3.0, 3.3, 3.0, and 2.2, respectively.

RGO support without functionalization (~7 nm). However, increasing the degree of functionalization of GO with PPD or BZD results in the formation of larger and less dispersed Pd nanoparticles on the surface of the functionalized GO support.

3.2. Suzuki coupling reaction

The catalytic activity of the prepared Pd catalysts (with Pd contents of 2.2 – 3.5 wt% as determined by ICP-MS) was investigated using the Suzuki cross coupling reaction of bromobenzene (0.32 mmol) and phenylboronic acid (0.38 mmol) with a 0.3 mol % Pd catalyst in a mixture of H_2O:C_2H_5OH (1:1) at room temperature (r.t.) according to Scheme 1.

Fig. 5 illustrates the % conversion of the room temperature reaction in Scheme 1 for different Pd catalysts supported on RGO and partially functionalized RGO with different contents of PPD

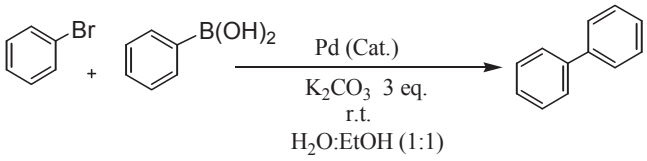

Scheme 1.

(Fig. 5-A) and BZD (Fig. 5-B). Fig. 5(A) clearly shows significantly higher conversions to the biphenyl product on the Pd/RGO-0.025 PPD and the Pd/RGO-0.05 PPD catalysts in reactions containing 0.22 and 0.24 mol% Pd, respectively than on the Pd/RGO catalyst in a reaction with 0.33 mol% Pd. The same trend is observed in Fig. 5(B) where the Pd/RGO-0.025 BZD, Pd/RGO-0.05 BZD and Pd/RGO-0.1 BZD catalysts in reactions involving 0.31, 0.33 and 0.28 mol% Pd, respectively have higher activity than the Pd/RGO catalyst in the same reaction containing 0.33 mol% Pd. These results are very significant since they demonstrate that the Suzuki reaction can be carried out within 15 min at room temperature yielding 94–95% of the biphenyl product using 0.2–0.3 mol% Pd of the Pd/RGO-0.025 PPD and the Pd/RGO-0.025 BZD catalysts, respectively.

The results in Fig. 5 also show that the Pd/RGO-0.1 BZD catalyst has higher activity than the Pd/RGO-0.1 PPD catalyst in the reaction that utilizes a similar Pd concentration of 0.28 mol%. For example, the Pd/RGO-0.1 BZD and the Pd/RGO-0.1 PPD catalysts exhibit 84% and 18% conversion, respectively after 15 min reaction time. Within 30 min, the GO-0.1 BZD catalyst effectively has attained nearly full (96%) conversion in comparison with the 65% conversion of the GO-0.1 PPD catalyst as shown in Fig. 5. It is also clear that the catalytic activity sharply decreases as the BZD or PPD content in the RGO support increases. For example, the Pd/RGO-0.025 BZD, Pd/RGO-0.05 BZD, Pd/RGO-0.1 BZD, Pd/RGO-0.2 BZD, and Pd/RGO-0.5 BZD catalysts utilizing Pd concentrations of 0.31, 0.33, 0.28, 0.26, and 0.21 mol%, respectively show product conversion ratios (within 15 min reaction time) of 93%, 95%, 82%, 22%, and 2%, respectively. It appears that the catalytic activity correlates with both the structure of the support and the Pd particle's size. Table 1 compares the 2Θ value of the XRD d_{001} peak of the support, the d-spacing of the support, the Pd particle size, the Pd wt% in the catalyst determined by ICP-MS, the Pd mol% used in the reaction, and the turnover frequency (TOF) values calculated after 15 min reaction time at room temperature.

In addition to the room temperature reactions, the catalysts were also evaluated for the reactions conducted under microwave irradiation (MWI) at 80 °C, and the results are shown in Table 2. At a lower catalyst concentration of 0.03 Pd mol%, the Pd/RGO-0.025 PPD and Pd/RGO-0.025 BZD catalysts yield the biphenyl product with conversions of 78% and 80%, respectively only after one minute reaction time as shown in Table 2. The two catalysts show almost a complete conversion (97–99%) to the biphenyl product while the Pd/RGO catalyst shows only 23% conversion after two-minute reaction time. Increasing the PPD or BZD content in the RGO support results in decreasing the catalytic activity consistent with the trend observed in the room temperature reactions. This is shown in the Pd/RGO-0.1 PPD and Pd/RGO-0.1 BZD catalysts, which exhibit 57% and 92% conversions, respectively after two-minute reaction time as compared to the nearly complete conversion to the biphenyl product displayed by the Pd/RGO-0.025 PPD and Pd/RGO-0.025 BZD catalysts using the same Pd concentration of 0.03 mol%. Again, the Pd/RGO-0.1 BZD catalyst shows higher activity than the Pd/RGO-0.1 PPD catalyst under similiar reaction conditions. Further reduction in the catalyst's concentration provided some insight into the reactivity of these two catalysts. Following the reaction under the same conditions (MWI, 80 °C) with the lowest Pd concentration of 0.007 mol%, the Pd/RGO-0.025 PPD and Pd/RGO-0.025 BZD catalysts led to conversions of 47.6% and 43.6%, respectively after one-minute reaction time. These results demonstrate the remarkable catalytic activity of the Pd/RGO-0.025 PPD and Pd/RGO-0.025 BZD catalysts with TOF values of 408,000 h^{-1} and 373,700 h^{-1}, respectively. To our knowledge, these are the highest TOFs observed in a microwave-assisted Suzuki cross coupling reaction by supported Pd nanoparticle catalysts [18].

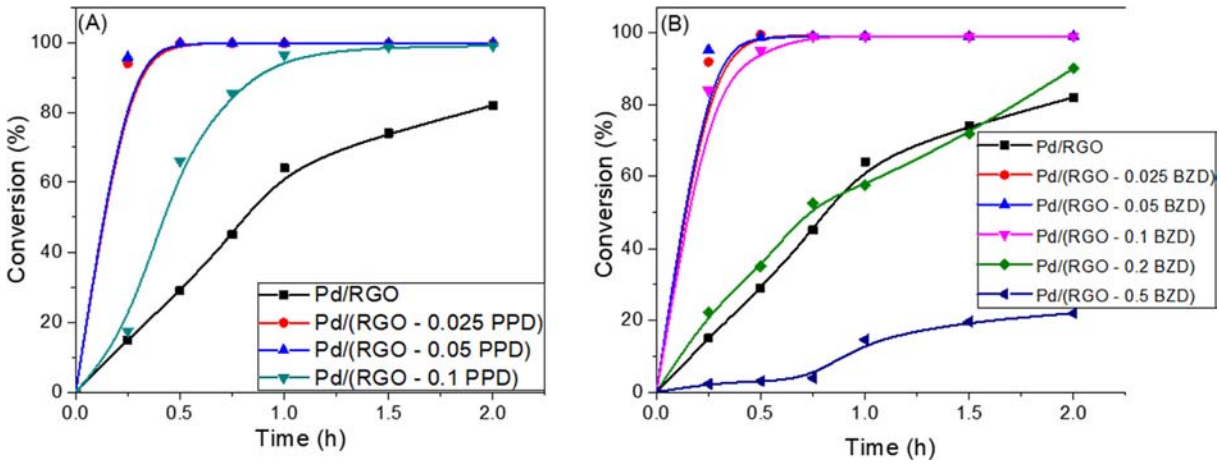

Fig. 5. % Conversion of the Suzuki cross-coupling reaction of (A) Pd/RGO and Pd/RGO- (0.025–0.1 mmol) PPD catalysts and (B) Pd/RGO and Pd/RGO-(0.025–0.5 mmol) BZD catalysts. Reaction conditions: 0.32 mmol bromobenzene, 0.38 mmol phenylboronic acid, 1 mmol K_2CO_3, and stirring speed of 450 rpm at room temperature with the Pd mol % of 0.33, 0.22, 0.24, 0.28, 0.31, 0.33, 0.28, 0.26, and 0.21 for the catalysts Pd/RGO, Pd/RGO-0.025 PPD, Pd/RGO-0.05 PPD, Pd/RGO-0.1 PPD, Pd/RGO-0.025 BZD, Pd/RGO-0.05 BZD, Pd/RGO-0.1 BZD, Pd/RGO-0.2 BZD, and Pd/RGO-0.5 BZD, respectively.

Table 1
Summary of Catalysts' Characterization and Performance. The 2Θ value of the XRD d_{001} peak of the support, the d-spacing of the support (nm), the Pd particle size (nm), the Pd wt % determined by ICP-MS in the catalyst, the Pd concentration used in the reaction (mol%), and the TOF values (h^{-1}) calculated after 15 min reaction time at room temperature.

Catalyst	2Θ (°)	d-Spacing (nm)	Pd Loading (wt%)	Pd Particle Size (nm)	Pd Concentration (mol%)	TOF (h^{-1})
Pd/RGO	11.3	0.78	3.5	7.1 ± 5	0.33	180
Pd/(RGO-0.025 PPD)	13.1	0.68	2.3	2.9 ± 0.7	0.22	1,740
Pd/(RGO-0.1 PPD)	7.3	1.21	3.0	2.7 ± 0.6	0.28	250
Pd/(RGO-0.025 BZD)	13.7	0.65	3.3	2.2 ± 1.1	0.31	1,230
Pd/(RGO-0.05 BZD)	13.3	0.66	3.5	4.3 ± 2.0	0.33	1,160
Pd/(RGO-0.1 BZD)	12.9	0.69	3.0	6.6 ± 5.6	0.28	870
Pd/(RGO-0.2 BZD)	11.3, 7.8	0.78, 1.13	2.8	7.5 ± 3.2	0.26	340
Pd/(RGO-0.5 BZD)	6.3	1.41	2.2	11.9 ± 19.9	0.21	45

Table 2
Conversion to the biphenyl product under MWI at 80 °C.

Catalyst	Pd mol%	Reaction Time (min)	Conversion (%)	TOF (h^{-1})
Pd/RGO	0.03	2	23.0	23,000
Pd/(RGO-0.025 PPD)	0.03	1	78.0	156,000
Pd/(RGO-0.025 PPD)	0.03	2	96.7	96,700
Pd/(RGO-0.025 BZD)	0.03	2	99.3	99,300
Pd/(RGO-0.1 PPD)	0.03	2	57.2	57,200
Pd/(RGO-0.1 BZD)	0.03	2	92.4	92,400
Pd/RGO	0.007	1	8.4	72,000
Pd/RGO	0.007	2	9.0	38,000
Pd/(RGO-0.025 PPD)	0.007	1	47.6	408,000
Pd/(RGO-0.025 PPD)	0.007	2	48.0	205,700
Pd/(RGO-0.025 BZD)	0.007	1	43.6	373,700
Pd/(RGO-0.025 BZD)	0.007	2	45.0	192,900

The results shown in Table 2 indicate that with the lowest catalyst concentration used of 0.007 Pd mol%, no change in the conversion % is observed within the one and two minute reaction times under the MW reaction conditions. This could be due to blocking of the catalyst active sites, as the amounts of the reactants are much more than the Pd active sites. This also indicates that the amount of the support plays an important role in the catalytic activity as it influences the surface area exposed to the reaction.

To generalize the above results, the range of catalytic utility in the Suzuki cross- coupling reactions for the preparation of other biphenyl products containing a broader range of functionality was investigated using the Pd/RGO-0.025 PPD catalyst. As illustrated in Table 3, the reactions were carried out in the presence of 0.03 Pd mol% under microwave heating at 80 ºC for 2 min. As shown in Table 3, a broad range of aryl bromide containing electron donating (methyl and methoxy), and electron withdrawing groups (nitrile and aldehyde) can be effectively incorporated in the coupling products.

3.3. Recycling of the catalysts

A significant practical application of heterogeneous catalysis is in the ability to easily remove the catalyst from the reaction mixture and reuse it for subsequent reactions until the catalyst is

Table 3
Evaluation of derivatives for the Suzuki cross-coupling reaction. Aryl bromide or iodide (0.32 mmol, 1 equiv), arylboronic acid (0.38 mmol, 1.2 equiv), potassium carbonate (1 mmol, 3 equiv), in 4 ml (1:1 H_2O–EtOH) was heated at 80 °C (MWI) for 2 min with 0.03 Pd mol% of the Pd/RGO-0.025 PPD catalyst. Conversion (%) was determined by GC–MS analysis.

Aryl bromide or iodide	Aryl boronic acid	Product	Conversion %
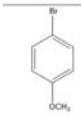		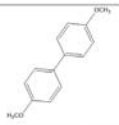	97.7 %
		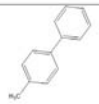	95.6 %
			100 %
		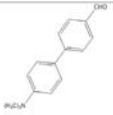	77.6 %
	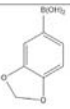	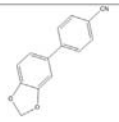	100 %
	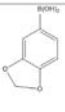	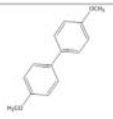	98.2 %

sufficiently deactivated. Thus, the ability to recycle the Pd/RGO-0.1 BZD catalyst was studied for the reaction of bromobenzene with phenylboronic acid utilizing 0.3 Pd mol% for 5 min reaction time using MWI at 80 °C. After the completion of the reaction, the mixture was diluted with 10 ml of EtOH and centrifuged and the solvent above the Pd catalyst was completely decanted. The EtOH washing followed by centrifugation was repeated two additional times to assure the removal of all the products from the catalyst surface. The catalyst was then directly transferred to another microwave tube along with fresh reagents for the next run. This procedure was repeated for every run and the percent conversion of product was determined by GC–MS as shown in Table 4. The Pd contents (wt%) in the spent catalysts after the first, second and sixth runs were also determined by ICP-MS as shown in Table 4.

As shown in Table 4, the Pd/RGO-0.1 BZD catalyst demonstrates nearly 100% conversion to the biphenyl product within the first four runs despite the decrease in the Pd content of the catalyst from 3 wt% to 2.93 wt% and 2.53 wt% after the first and second runs, respectively. The loss of Pd is most likely due to the dissolution of the very small Pd nanoparticles during the extensive washing and centrifuging of the catalyst in order to remove the reaction products from the surface of the catalyst after each reaction run. This is also confirmed by the ICP-MS analysis of the reaction solution after the removal of the catalyst, which shows that the palladium content in the solution is only 200–250 ppb. Such a small amount of leached palladium support the heterogeneity of the catalytic system in this reaction. Further evidence on the heterogeneous nature of the catalytic mechanism is the failure to observe reactivity in the room temperature reaction after the removal of the Pd/RGO-0.1 BZD catalyst by hot filtration from the reaction medium after 10 min of the reaction where 45% conversion to the biphenyl product had already been achieved.

Table 4
Recycling and ICP analysis of the Pd/RGO-0.1BZD catalyst containing 3 wt% Pd. Conditions: 0.3 mol% Pd, 0.32 mmol bromobenzene, 0.38 mmol phenylboronic acid, 1 mmol K_2CO_3. Microwave Irradiation: 300 W, 80 °C, 5 min reaction time.

Reaction Cycle	Conversion (%)	Pd (wt%) ICP
1	100	2.93
2	99	2.53
3	99	–
4	97	–
5	86	–
6	82	2.31

4. Discussion

The extent of the enhanced catalytic activity of the supported Pd nanoparticles as described above depends on the degree of loading of the aromatic molecules into the RGO support. At very low loadings of PPD and BZD (0.025 mmol) as in the Pd/(RGO-0.025 PPD) and Pd/(RGO-0.025 BZD) catalysts, the interlayer spacing between the RGO sheets did not change much from the 0.8 nm of GO resulting in an XRD peak at 2θ = 11.0° [34,46]. However, at higher loadings of PPD (0.6 mmol) and BZD (0.5 mmol), d spacing of 1.2 nm and 1.4 nm were observed, respectively as shown in Fig. 3, and a significant decrease in the catalyst activity of these catalysts was observed.

The low loading of PPD and BZD results in a partial functionalization of the GO support which is critical for the strong electrostatic adsorption of the cationic Pd precursor. Partial functionalization entails a greater abundance of oxygen groups, whereas full reduction of GO eliminates the oxygen groups on the surface of GO [10]. A higher degree of intact oxygen groups on the GO surface allows SEA uptake of cationic palladium salts, leading to smaller Pd particle's size because such functional groups act as nucleation sites, and a higher content of oxygen groups leads to a higher nucleation rate [36–39]. However, complete functionalization of GO with the aromatic amines results in nearly total reduction of GO, which eliminates most of the oxygen groups present on the surface needed for the strong electrostatic adsorption of the Pd cations. This leads to less effective nucleation sites on the surface and enhances the growth and aggregation of the Pd nanoparticles.

Fig. 6 illustrates the concept of partial and full functionalization of GO by PPD. Oxygen-containing groups on the surface of graphene oxide are directly responsible for the spacing of GO layers as shown in Fig. 6A. Their removal by reductive functionalization agents such as PPD results in the inevitable restacking of graphitic layers, and a decrease in the d-spacing is expected [46,47]. When GO is only partially reduced/functionalized by such aromatic amines, the GO layers collapse due to the removal of oxygen groups, as illustrated in Fig. 6B. In this case, there is an insufficient quantity of bulky aromatic amine spacers to act as scaffolding to replace the reduced oxygen groups, leading to non-uniform spacing as observed in the XRD patterns obtained by the low loading of PPD or BZD. This phenomenon has previously been attributed to irregular interlayer spacing due to disorderly bonding [27,28]. However, at a higher loading of PPD, a d-spacing of 1.2 nm can be achieved for the RGO-PPD composite as illustrated in Fig. 6C. It has been reported that a molecular density of intercalant agent needs to be at least 25 wt% to achieve exfoliation of d-spacing to 1.4 nm [28,29].

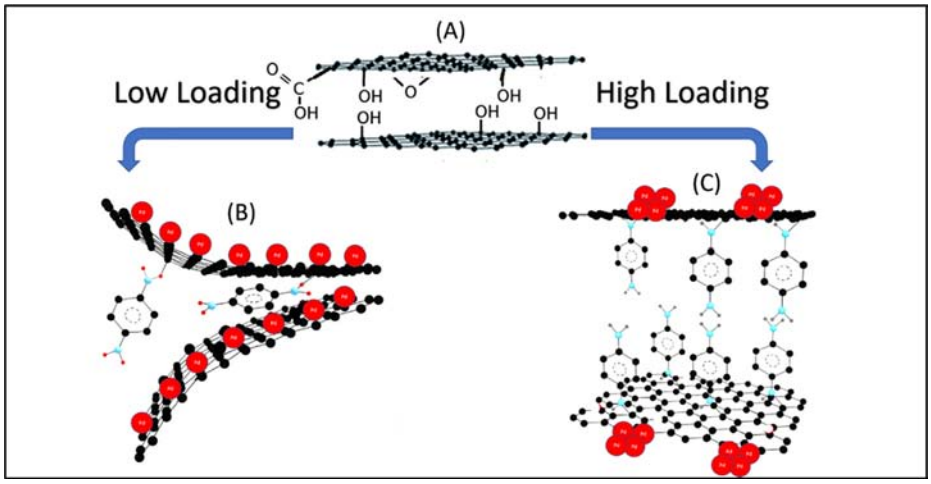

Fig. 6. Illustration of GO (A) followed by subsequent reduction/functionalization with a high concentration of *p*-phenylenediamine yielding increased spacing (B) or low concentration of *p*-pheneylenediamine yielding irregular spacing (C).

As shown in Table 1, a decrease in the actual Pd% loading on the support is observed when a higher BZD concentration is used resulting in complete substitution of the oxygen groups by the amine moieties. For example, the Pd wt% in the Pd/(RGO-0.025 BZD), Pd/(RGO-0.1 BZD), Pd/(RGO-0.2 BZD), and Pd/(RGO-0.5 BZD) catalysts are determined to be 3.3, 3.0, 2.8, and 2.2 wt%, respectively. A higher BZD loading in the RGO support leads to lower oxygen availability in the support, which results in fewer palladium cations electrostatically adsorbed onto the GO via strong attraction to the oxygen functional groups. Therefore, less nucleation events and more particle's growth are favoured at higher concentrations of the aromatic amine functionalization. The TEM images of the supported Pd catalysts provide strong evidence for the effect of partial functionalization and reduction of the GO support by the aromatic amines on the size distribution of the Pd nanoparticles. As shown in Fig. 4, the average size of the Pd nanoparticles increases from 2.2 ± 1.1 to 6.6 ± 5.6 to 11.9 ± 19.9 n m as the BZD content in the RGO support increases from 0.025 to 0.1 to 0.5 mmol. Table 1 shows that the drop in the catalytic activity is directly correlated with increasing the size and size distribution of the Pd nanoparticles. As the oxygen content on the RGO support is displaced by the nucleophilic substitution of the bulky aromatic amine groups, there is less oxygen for the strong electrostatic adsorption of the cationic Pd precursors, leading to fewer seeds and more aggregation of nanoparticles on the support. Table 1 also shows a decrease in the actual Pd% loading as a higher BZD concentration is incorporated into the RGO support where the oxygen groups are completely substituted by amine moieties. These results are consistent with the generally accepted trend that the introduction of oxygenated surface groups on a carbon-based support, particularly carboxylic groups, results in catalysts with higher metal loadings and dispersions [48–50].

In addition to coordinating the cationic palladium precursors, the presence of amines is believed to assist in the reduction of palladium ions. The XPS results (Fig. 2C) show higher % Pd(0) for the Pd/RGO-0.1 BZD catalyst (37%) compared to the Pd/RGO-0.1 PPD (31%) and the Pd/RGO (27%) catalysts. Therefore, it appears that the degree of the aromatic amine functionalization of GO could tune both the Pd particle size and the % of Pd(0) on the functionalized support, which would in turn affect the catalytic activity of the supported catalyst. The extraordinary catalytic activity of the Pd/(RGO- 0.025 PPD) and (Pd/RGO-0.025 BZD) catalysts could be attributed to enhancing the strong electrostatic adsorption of the cationic Pd precursors through complexation with the oxygen and amine functional groups of the partially functionalized support which could improve the dispersion of the Pd nanoparticles formed after the reduction of the Pd ions. The assisted reduction of GO by the aromatic amines is also expected to restore or partially restore the sp^2 domains which could lead to extending the electron conjugation between the sp^2 domains of RGO and the aromatic amines thus facilitating the charge flow mechanism in cross-coupling reactions [15,20]. The extended π-system and high π-electron density of the covalently functionalized RGO support with PPD and BZD could assist electron flow between the Pd nanoparticles and the support. In fact, previous work has shown that covalent functionalization of GO with PPD results in nearly 9 orders of magnitude higher electrical conductivity than that of GO [26]. The excellent electrochemical features of the RGO-PPD composite including the very high specific capacitance have been attributed to rapid charge transport and low charge transfer resistance across the composite [28]. Therefore, the covalent attachment of the electron-rich aromatic amines to the surface of RGO can alter the donor characteristics of the support, facilitate the charge exchange and reduce the sintering of the Pd nanoparticles.

5. Conclusions

In conclusion, highly active palladium nanoparticle catalysts supported on partially functionalized reduced graphene oxide with aromatic amines have been developed for Suzuki coupling reactions. The partial functionalization of the reduced graphene oxide support with *p*-phenylenediamine or benzidine allows the retention of oxygen groups along with nitrogen-containing groups on the support which results in strong electrostatic adsorption and coordination of the of the cationic palladium precursor and assisted reduction leading to well-dispersed small Pd nanoparticles. The highest catalytic is observed for catalysts supported on reduced graphene oxide with minimal amounts of aromatic amine functionalization. These catalysts exhibit unprecedented catalytic activity that surpasses the performance of Pd catalysts supported on other carbon-based supports and matches that of the best homogeneous Pd catalysts for the Suzuki cross-coupling reactions.

Declaration of Competing Interest

The authors declare that they have no known competing financial interests or personal relationships that could have appeared to influence the work reported in this paper.

Acknowledgments

We thank the National Science Foundation (CHE-1900094) for the support of this work. This work was also partially supported by the Center for Rational Catalysis Synthesis (CeRCaS), an Industry/University Cooperative Research Center funded in part by the National Science Foundation [Industry/University Collaborative Research Center grant IIP1464595].

Appendix A. Supplementary material

Supplementary data to this article can be found online at https://doi.org/10.1016/j.jcat.2020.03.011.

References

[1] A. Schaetz, M. Zeltner, W.J. Stark, Carbon in catalysis, ACS Catal. 2 (2012) 1267–1284.
[2] D.S. Su, S. Perathoner, G. Centi, Nanocarbons for the development of advanced catalysts, Chem. Rev. 113 (2013) 5782–5816.
[3] H. Xiong, L.L. Jewell, N.J. Coville, Shaped carbons as supports for the catalytic conversion of syngas to clean fuels, ACS Catal. 5 (2015) 2640–2658.
[4] Á. Molnár, Efficient, selective, and recyclable palladium catalysts in carbon−carbon coupling reactions, Chem. Rev. 111 (2011) 2251–2320.
[5] A. Fihri, M. Bouhrara, B. Nekoueishahraki, J.M. Basset, V. Polshettiwar, Nanocatalysts for Suzuki cross-coupling reactions, Chem. Soc. Rev. 40 (2011) 5181–5203.
[6] H. Li, C.C.J. Seechurn, T.J. Colacot, Development of preformed Pd catalysts for cross-coupling reactions, beyond the 2010 nobel prize, ACS Catal. 2 (2012) 1147–1164.
[7] M. Pagliaro, V. Pandarus, R. Ciriminna, F. Béland, P. Demma Carà, Heterogeneous versus homogeneous palladium catalysts for cross-coupling reactions, ChemCatChem 4 (2012) 432–445.
[8] G.M. Scheuermann, L. Rumi, P. Steurer, W. Bannwarth, R. Mülhaupt, Palladium nanoparticles on graphite oxide and its functionalized graphene derivatives as highly active catalysts for the Suzuki−Miyaura coupling reaction, J. Am. Chem. Soc. 131 (2009) 8262–8270.
[9] A.R. Siamaki, A.E.R.S. Khder, V. Abdelsayed, M.S. El-Shall, B.F. Gupton, Microwave-assisted synthesis of palladium nanoparticles supported on graphene: A highly active and recyclable catalyst for carbon-carbon cross-coupling reactions, J. Catal. 279 (2011) 1–11.
[10] S. Moussa, A.R. Siamaki, B.F. Gupton, M.S. El-Shall, Pd-partially reduced graphene oxide catalysts (Pd/PRGO): laser synthesis of Pd nanoparticles supported on PRGO nanosheets for carbon-carbon cross coupling reactions, ACS Catal. 2 (2012) 145–154.
[11] Y. Nishina, J. Miyata, R. Kawai, K. Gotoh, Recyclable Pd-graphene catalyst: mechanistic insights into heterogeneous and homogeneous catalysis, RSC Adv. 2 (2012) 9380–9382.
[12] A.R. Siamaki, Y. Lin, K. Woodberry, J.W. Connell, B.F. Gupton, Palladium nanoparticles supported on carbon nanotubes from solventless preparations: versatile catalysts for ligand-free suzuki cross coupling reactions, J. Mater. Chem. A 1 (2013) 12909–12918.
[13] H.A. Elazab, A.R. Siamaki, S. Moussa, B.F. Gupton, M.S. El-Shall, Highly efficient and magnetically recyclable graphene-supported Pd/Fe_3O_4 nanoparticle catalysts for suzuki and heck cross-coupling reactions, Appl. Catal. A 491 (2015) 58–69.
[14] H.A. Elazab, S. Moussa, A.R. Siamaki, B.F. Gupton, M.S. El-Shall, The effect of graphene on catalytic performance of palladium nanoparticles decorated with Fe_3O_4, Co_3O_4, and $Ni(OH)_2$: potential efficient catalysts used for Suzuki cross coupling reactions, Catal. Lett. 147 (2017) 1510–1522.
[15] Y. Yang, A.C. Reber, S.E. Gilliland III, C.E. Castano, B.F. Gupton, S.N. Khanna, More than just a support: graphene as a solid-state ligand for palladium-catalyzed cross-coupling reactions, J. Catal. 2018, 360, 20–26.
[16] J.A. Bobb, A.A. Ibrahim, M.S. El-Shall, Laser synthesis of carbonaceous TiO_2 from metal-organic frameworks: optimum support for Pd nanoparticles for C-C cross-coupling reactions, ACS Appl. Nano Mater. 1 (2018) 4852–4862.
[17] X. Zhang, Z. Sun, B. Wang, Y. Tang, L. Nguyen, Y. Li, F.F. Tao, C−C Coupling on single-atom-based heterogeneous catalyst, J. Am. Chem. Soc. 140 (2018) 954–962.
[18] Z. Chen, E. Vorobyeva, S. Mitchell, E. Fako, M.A. Ortuno, N. Lopez, S.M. Collins, P.A. Midgley, S. Richard, G. Vile, A heterogeneous single-atom palladium catalyst surpassing homogeneous systems for suzuki coupling, Nat. Nanotechnol. 13 (2018) 702–707.
[19] S.O. Moussa, L.S. Panchakarla, M.Q. Ho, M.S. El-Shall, Graphene-supported, iron-based nanoparticles for catalytic production of liquid hydrocarbons from synthesis gas: the role of the graphene support in comparison with carbon nanotubes, ACS Catal. 4 (2014) 535–545.
[20] Y. Yang, C.E. Castano, B.F. Gupton, A.C. Reber, S.N. Khanna, A fundamental analysis of enhanced cross-coupling catalytic activity for palladium clusters on graphene supports, Nanoscale 8 (2016) 19564–19572.
[21] F. Banhart, J. Kotakoski, A.V. Krashennnikov, Structural defects in graphene, ACS Nano 5 (2011) 26–41.
[22] G. Kim, S.-H. Jhi, Carbon monoxide-tolerant platinum nanoparticle catalysts on defect-engineered graphene, ACS Nano 5 (2011) 805.
[23] Tri Truong-Huu, Kambiz Chizari, Izabela Janowska, Maria Simona Moldovan, Ovidiu Ersen, Lam D. Nguyen, Marc J. Ledoux, Cuong Pham-Huu, Dominique Begin, Few-layer graphene supporting palladium nanoparticles with a fully accessible effective surface for liquid-phase hydrogenation reaction, Catal. Today 189 (2012) 77–82.
[24] Xiaoqi Chen, Dehui Deng, Xiulian Pan, Yongfeng Hu, Xinhe Bao, N-doped graphene as an electron donor of iron catalysts for CO hydrogenation to light olefins, Chem. Comm. 51 (2015) 217–220.
[25] Yi Cheng, Jun Lin, Xu. Ke, Hao Wang, Xuanyu Yao, Yan Pei, Shirun Yan, Minghua Qiao, Baoning Zong, Fischer-Tropsch synthesis to lower olefins over potassium-promoted reduced graphene oxide supported iron catalysts, ACS Catal. 6 (2016) 389–399.
[26] H.-L. Ma, H.B. Zhang, Q.H. Hu, W.J. Li, Z.G. Jiang, Z.Z. Yu, A. Dasari, Functionalization and reduction of graphene oxide with *p*-phenylenediamine for electrically conductive and thermally stable polystyrene composites, ACS Appl. Mater. Interfaces 4 (2012) 1948–1953.
[27] W.S. Hung, C.H. Tsou, M. De Guzman, Q.F. An, Y.L. Liu, Y.M. Zhang, C.C. Hu, K.R. Lee, J.Y. Lai, Cross-linking with diamine monomers to prepare composite graphene oxide-framework membranes with varying d-spacing, Chem. Mater. 26 (2014) 2983–2990.
[28] B. Song, J.I. Choi, Y. Zhu, Z. Geng, L. Zhang, Z. Lin, C. Tuan, K. Moon, C. Wong, Molecular level study of graphene networks functionalized with phenylenediamine monomers for supercapacitor electrodes, Chem. Mater. 28 (2016) 9110–9121.
[29] E.C. Vermisoglou, T. Giannakopoulou, G. Romanos, N. Boukos, V. Psycharis, C. Lei, C. Lekakou, D. Petridis, C. Trapalis, Graphene-based materials via benzidine-assisted exfoliation and reduction of graphite oxide and their electrochemical properties, Appl. Surf. Sci. 392 (2017) 244–255.
[30] T.P.N. Tran, A. Thakur, D.X. Trinh, A.T.N. Dao, T. Taniike, Design of Pd@graphene oxide framework nanocatalyst with improved activity and recylability in Suzuki-Miyaura cross-coupling reaction, Appl. Catal. A. 549 (2018) 60–67.
[31] S.E. Gilliland, J.M.M. Tengco, Y. Yang, J.R. Regalbuto, C.E. Castano, B.F. Gupton, Electrostatic adsorption-microwave synthesis of palladium nanoparticles on graphene for improved cross-coupling activity, Appl. Catal. A. 550 (2018) 168–175.
[32] A. Wong, Q. Liu, S. Griffin, A. Nicholls, J.R. Regalbuto, Synthesis of ultrasmall, homogeneously alloyed, bimetallic nanoparticles on silica supports, Science 358 (2017) 1427–1430.
[33] W.S. Hummers Jr., R.E. Offeman, Preparation of graphitic oxide, J. Am. Chem. Soc. 80 (1958), 1339–1339.
[34] V. Abdelsayed, S. Moussa, H.M. Hassan, H.S. Aluri, M.M. Collinson, M.S. El-Shall, Photothermal deoxygenation of graphite oxide with laser excitation in solution and graphene-aided increase in water temperature, J. Phys. Chem. Lett 1 (2010) 2804–2809.
[35] L. Jiao, J.R. Regalbuto, The synthesis of highly dispersed noble and base metals on silica via strong electrostatic adsorption: II. Mesoporous silica SBA-15, J. Cat. 260 (2008) 342–350.
[36] L. Dsouza, J.R. Regalbuto, Strong electrostatic adsorption for the preparation of Pt/Co/C and Pd/Co/C bimetallic electrocatalysts, in: E.M. Gaigneaux, M. Devillers, S. Hermans, P.A. Jacobs, J.A. Martens, P. Ruiz (Eds.), Studies in Surface Science and Catalysis, Vol. 175, Elsevier, 2010, pp. 715–718.
[37] L. D'Souza, L. Jiao, J.R. Regalbuto, J.T. Miller, A.J. Kropf, Preparation of silica- and carbon-supported cobalt by electrostatic adsorption of Co(III) hexaammines, J. Cat. 248 (2007) 165–174.
[38] X. Hao, S. Barnes, J.R. Regalbuto, A fundamental study of Pt impregnation of carbon: adsorption equilibrium and particle synthesis, J. Cat. 279 (2011) 48–65.
[39] G.S. Seuser, R. Banerjee, K. Metavarayuth, A.J. Brandt, T.D. Maddumapatabandi, S. Karakalos, Y. Lin, J.R. Regalbuto, D.A. Chen, Understanding uptake of Pt precursors during strong electrostatic adsorption on single-crystal carbon surfaces, Top. Catal. 61 (2018) 379–388.
[40] F.T. Johra, J.-W. Lee, W.-G. Jung, Facile and safe graphene preparation on solution based platform, Ind. Eng. Chem. Res. 20 (2014) 2883–2887.
[41] A.H. Labulo, B.S. Martincigh, B. Omondi, V.O. Nyamori, Advances in carbon nanotubes as efficacious supports for palladium-catalysed carbon-carbon cross-coupling reactions, J. Mat. Sci. 52 (2017) 9225–9248.
[42] G.A. Molander, T. Fumagalli, Palladium(0)-catalyzed Suzuki−Miyaura cross-coupling reactions of potassium aryl- and heteroaryltrifluoroborates with alkenyl bromides, J. Org. Chem. 71 (2006) 5743–5747.
[43] A. Mahanta, N. Hussain, R. Das Manash, J. Thakur Ashim, U. Bora, Palladium nanoparticles decorated on reduced graphene oxide: an efficient catalyst for ligand- and copper-free sonogashira reaction at room temperature, Appl. Organometallic Chem. 31 (2017) e3679.
[44] B.J. Reizman, Y.-M. Wang, S.L. Buchwald, K.F. Jensen, Suzuki-Miyaura cross-coupling optimization enabled by automated feedback, React. Chem. Eng. 1 (2016) 658–666.
[45] W. Ai, W. Zhou, Z. Du, Y. Du, H. Zhang, X. Jia, L. Xi, M. Yi, T. Yu, W. Huang, Benzoxazole and benzimidazole heterocycle-grafted graphene for high-performance supercapacitor electrodes, J. Mat. Chem. 22 (2012) 23439–23446.
[46] F.S. Awad, H.D. Kiriarachchi, K.M. AbouZeid, Ü. Özgür, M.S. El-Shall, Plasmonic graphene polyurethane nanocomposites for efficient solar water desalination, ACS Appl. Energy Mater. 1 (2018) 976–985.

[47] Y. Wang, Y. Wu, Y. Huang, F. Zhang, X. Yang, Y. Ma, Y. Chen, Preventing graphene sheets from restacking for high-capacitance performance, J. Phys. Chem. C 115 (2011) 23192–23197.
[48] S.D. Jin, P. Tae-Jin, I. Son-Ki, Effect of surface oxygen groups of carbon supports on the characteristics of Pd/C catalysts, Carbon 31 (1993) 427–435.
[49] M.C. Román-Martínez, D. Cazorla-Amorós, A. Linares-Solano, C.S.M. De Lecea, H. Yamashita, M. Anpo, Metal-support interaction in Pt/C catalysts, influence of the support surface chemistry and the metal precursor, Carbon 33 (1995) 3–13.
[50] S. Pang, Y. Zhang, Y. Huang, H. Yuan, F. Shi, N/O-doped carbon as a "Solid Ligand" for Nano-Pd catalyzed biphenyl- and triphenylamine syntheses, Catal. Sci. Tech. 7 (2017) 2170–2182.